

Hysteresis in Flutter

*T. Chandra Sekar¹⁾, Alakesh Chandra Mandal²⁾ and Abhijit Kushari³⁾

^{1), 2), 3)} Department of Aerospace Engineering, IIT Kanpur, Kanpur 208-016, India

¹⁾ tchandra@iitk.ac.in

ABSTRACT

An aeroelastic model of NACA0015 airfoil has been tested in a low speed wind tunnel. Kinematic parameters of the wing section and the aerodynamic parameters over the wing section were measured. During the experiment, the wind speed was increased from zero until the system underwent violent oscillations (flutter). The behavior of aerodynamic forces and moments on the wing section was found to exhibit hysteresis. The orientation of the hysteresis loop was found to undergo change as the wind speed was increased and the wing section encountered flutter. On comparing with the classical vibration problem, the change in orientation of hysteresis loop was related to the change in damping coefficient.

1. INTRODUCTION

Flutter is a dynamic aeroelastic problem which leads to the catastrophic failure of the structure moving in fluid. Civil and Aero structures like bridges, airplane wings, propeller blades etc. are prone to flutter if the aeroelastic parameters are not considered during the design phase. In depth understanding the dynamics of the flutter is essential for better designs and to implement control techniques.

Flutter arises due to the interaction of aerodynamic, elastic and inertia forces, well shown by "Collar triangle". In reality, flutter is manifested as the vibration of the structure moving in a fluid. Hence, as an immediate response, the engineer tends to use the governing equation for a classical vibration system as given by Eq. (1), where m , c and k are constants and $F(t)$ is external force acting on the system.

$$m\ddot{X} + c\dot{X} + kX = F(t) \quad (1)$$

For an aeroelastic system, the aerodynamic force and moment (constitutes the external force) acting on the structure depends on the position and orientation of the

¹⁾ Graduate Student

²⁾ Assistant Professor

³⁾ Professor

structure. The governing equation of the aeroelastic system is given by Eq. (2), where m , c and k are constants and $G(\ddot{X}, \dot{X}, X, t)$ is the aerodynamic force or moment.

$$m\ddot{X} + c\dot{X} + kX = G(\ddot{X}, \dot{X}, X, t) \quad (2)$$

For an aeroelastic system, the wind speed is embedded in the function G and is the control parameter. The behavior of the system changes with change in wind speed. At a particular wind speed called “flutter speed”, the output variable/dynamical variable(X) grows monotonically with time resulting in large amplitude oscillations. These large amplitude oscillations may induce stresses larger than the maximum value leading to the abrupt failure of the structure.

From Eq. (1) and Eq. (2) it is clear that the nature of right hand side of the equation differentiates (forcing function) the aeroelastic system from classical vibration system. For an aeroelastic system, the external force acting on the system depends on the system output. Understanding the behavior of the aerodynamic force and moment is crucial for estimating the flutter speed.

One of the first analytical works was carried out by Theodorsen (1941) for coupled mode flutter. The theory proposed by Theodorsen results in a mathematical equation for lift and moment acting on an airfoil mounted on one linear and one torsion spring, and is applicable only at the border case of flutter. It does not consider the transient response of the aeroelastic system or the behavior of the system beyond the flutter speed.

Other works pertinent here is by Lee and Gerontakos (2004), in which flow over an oscillating airfoil was studied. The key observation from their work is hysteresis loop formed by coefficients of lift, drag and moment with the airfoil motion. Based on this, the role of hysteresis on flutter behavior can be anticipated.

Moreover, the experimental investigation by Bolland and Brown (1941), indicates that the damping behavior of the aeroelastic system changes with wind speed. The work by Sekar et. al (2017) attempted to study the behavior of aeroelastic system beyond flutter speed and found to undergo second bifurcation.

The present experimental investigation aids in understanding the behavior of the aerodynamic forces and moments in the neighborhood of flutter speed. In the current work, an attempt has been made to understand the hysteresis behavior of the aeroelastic system. From the perspective of the system damping, the relationship between the classical vibration system (Eq. (1)) and the aeroelastic system (Eq. (2)) is presented.

2. EXPERIMENTAL SETUP, PROCEDURE AND DATA REDUCTION

The experiments were carried out in a low speed wind tunnel designed and developed at Indian Institute of Technology Kanpur, India.

2.1 Experimental Setup and instrumentation

The experimental model is used in the current study, and the experimental model placed in the wind tunnel are shown in Fig. 1(a) and Fig. 1(b) respectively. The “equivalent system” for easier mathematical representation is shown in Fig. 1(c). More details regarding the experimental setup and instrumentation can be found in reference by Sekar et. al. 2017.

The picture of the “experimental model” is shown in Fig. 1(a). The model consists of a wing section of NACA0015 profile, mounted on eight extension springs as shown. The values of various parameters of the model are listed in Table I. Figure 1(b) shows the picture of the experimental model placed in wind tunnel. For the present case the angle of attack is equal to zero. The Pitot-static probe is used to measure the wind speed at the inlet of the test-section.

Figure 1(c) shows the “equivalent system”, for better mathematical representation of the complex model (Fig. 1(a)). The eight spring forces acting on the experimental model is reduced to one force (linear spring) and one moment (torsional spring). This also helps to correlate the present experimental model to earlier works (using one compression and one torsion spring). In the equivalent system, eight extension springs are reduced to one compression spring and one torsion spring, with equivalent spring constants K_h and K_θ , respectively. These equivalent spring constants were obtained by force and moment balance. Hence, the complex motion of the wing section has been represented as heaving motion (h) along Z-axis and pitching motion (θ) about Y-axis.

Table 1: Parameter values related to aeroelastic system

Parameter		Value
Airfoil profile		NACA0015
Mass of wing		1.146 kg
Wing span (S)		0.325 m
Wing chord (C)		0.254 m
Spring constant (K)		27 N/m
Distance between springs		0.27 m
Static angle of attack (θ_0)		0°
Distance between C.G and E.A		0 m
Equivalent compression spring (K_h)		216 N/m
Equivalent torsion spring (K_θ)		29.16 N-m/rad
Damped Natural Frequency	Heaving	2.1 Hz
	Pitching	4.0 Hz

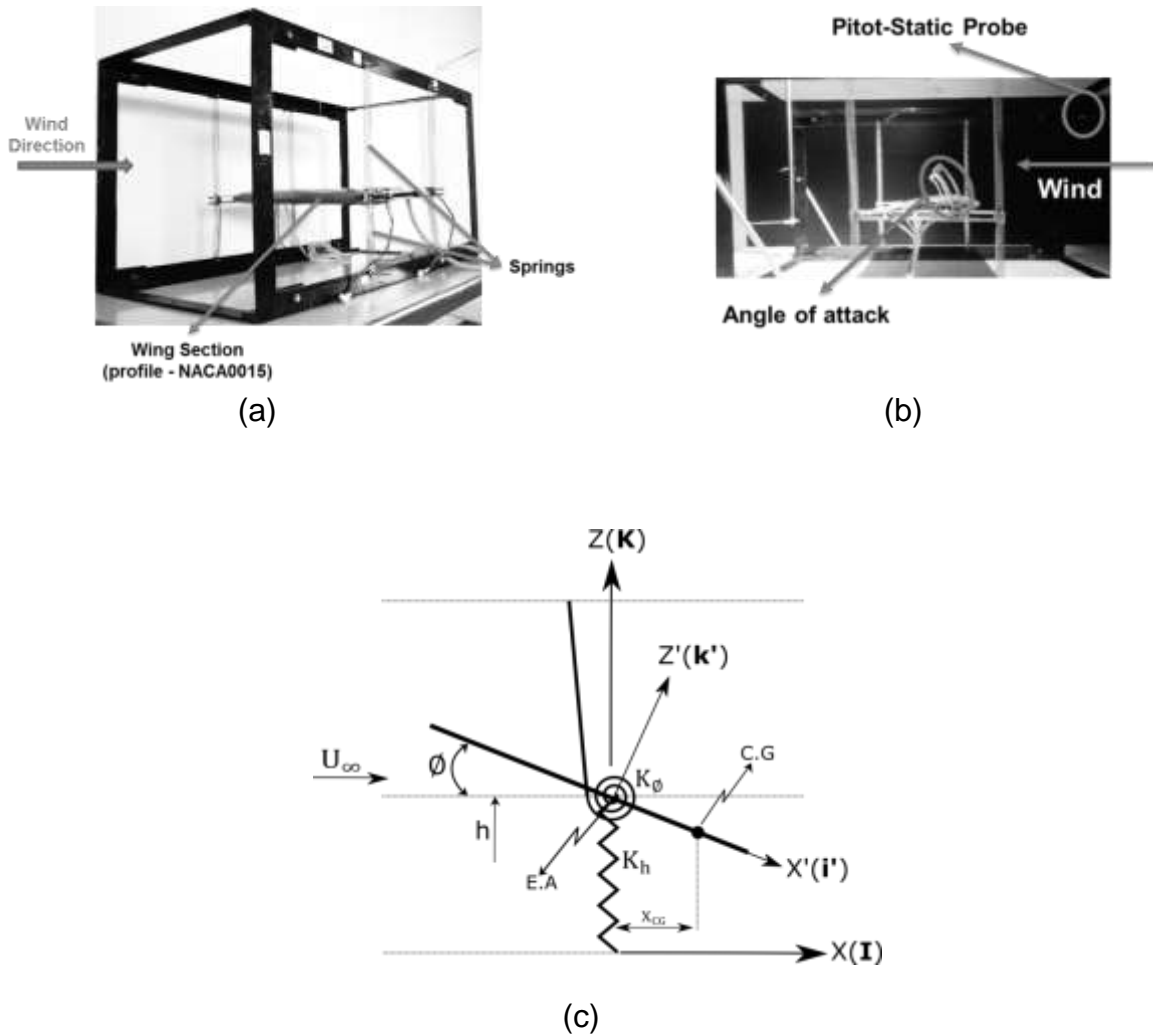


Fig. 1 (a) Picture of experimental model (b) Picture of experimental model placed in wind tunnel (c) Schematic of the “equivalent system”

In the current work, pressure along the surface of the wing was measured using a two ESP pressure scanner having 32 ports each and the incoming wind speed was measured using a Pitot-static probe. The full measurement span of the ESP scanner is equal to ± 4976 Pa (1 psi) with an accuracy of 0.03 % of full scale. The data were recorded at the rate of 250 samples per second from each pressure port.

The motion of the airfoil was found by tracking six bright circular dots pasted on the wing section using a video recorder. Video of the entire experiment was recorded at the rate of 50 frames per second. Later the video was converted into images and the location of the circular dots was computed by processing the image.

2.2 Experiment Procedure

The entire “experimental model” was placed in a low speed wind tunnel. Using a standard data acquisition system the data from all the sensors were recorded

continuously until the end of the experiment. After ensuring the proper functioning of sensors and the acquisition system, the wind speed was increased slowly until the wing undergoes flutter. As the behavior of the system depends on the wind speed (U_∞), detailed information related to the variation of the wind speed during the entire experiment is required. Figure 4 show the variation U_∞ of with time. The black line in the plot corresponds to U_∞ computed from every sample of the data, and the orange line corresponds to trends in U_∞ and given by mathematical forms in Table 2.

For the current analysis, the time interval $240s \leq t \leq 376s$ is of interest (shown as “Time of Interest (TOI)” in the Fig. 2). The wind speed (U_∞) variation in mathematical form is shown in Table 2.

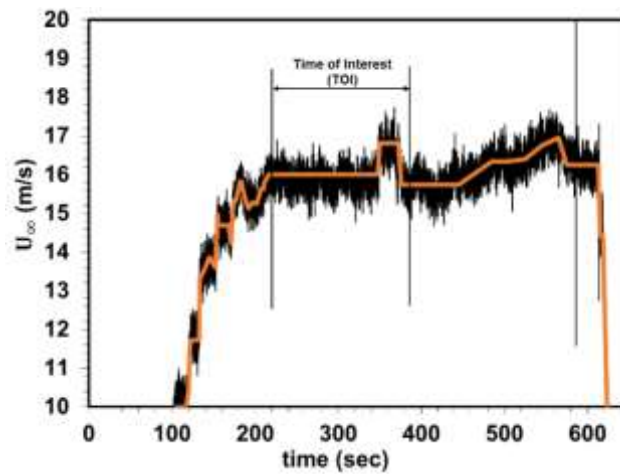


Fig. 2 Variation of wind speed (U_∞) with time

Table 2: Variation of wind speed in Time of Interest (TOI)

Time Interval	U_∞	Name
$217 \leq t \leq 347.5$	16.0 m/s	T1
$347.5 \leq t \leq 350$	$0.324t + -96.59$ m/s	T2
$350 \leq t \leq 372$	16.81 m/s	T3
$372 \leq t \leq 376$	$-0.266t + 116.32$ m/s	T4
$376 < t < 445$	15.74 m/s	T5

2.3 Data Reduction

Magnitude of lift (L) is estimated using Eq. (3), and magnitude of aerodynamic moment at E.A about Y-axis (M) is estimated using Eq. (4).

$$L = \cos\phi \sum_{i=1}^{NE} A_i P_i (\hat{\mathbf{n}}_i \cdot \mathbf{k}') - \sin\phi \sum_{i=1}^{NE} A_i P_i (\hat{\mathbf{T}}_i \cdot \mathbf{k}') \quad (3)$$

$$M = \sum_{i=1}^{NE} A_i P_i (\mathbf{r}_i \times \hat{\mathbf{n}}_i) \cdot \mathbf{J} \quad (4)$$

where 'NE' is the number of pressure ports available for measurement on the entire airfoil, $\hat{\mathbf{n}}_i$ is the unit normal vector to the airfoil surface at 'i', $\hat{\mathbf{T}}_i$ is the unit tangential vector to the airfoil surface at 'i' and A_i is the area of the i^{th} element on which the pressure P_i is acting, with the assumption that, uniform pressure (P_i) is acting over the element and the pressure (P_i) is being measured at the midpoint of the element. The lift L and moment (M) computed using Eq. (3) and Eq. (4) respectively, is filtered using low pass, Butterworth filter with cutoff frequency equal to 20 Hz to remove noise. The cutoff frequency was decided based on the oscillation frequency and the order of the filter was chosen to minimize the distortion of the processed signal.

The heaving and pitching displacement were computed by processing the images obtained from the video using video camera. The location of the circles (in pixels) in the images was found and the line passing through the circles were computed. The location of the center of the circles and its angle with respect to the horizontal were computed. Using the calibration image, heaving and pitching displacement were computed. After the displacements were computed, the data was resampled to 250 Hz by linear interpolation technique, in order to match with the data acquired using ESP scanner.

3. RESULTS AND DISCUSSION

Figure 3 shows the behavior of heaving and pitching displacement of the wing section along with wind speed (U_∞) during Time of Interest (TOI). During TOI, the following observations can be made regarding the behavior of wing section.

During T1, irregular intermittent oscillations along both heaving and pitching directions can be observed from Fig. 3(a) and Fig. 3(b) respectively. Amplitude of both heaving and pitching oscillations grow and decay simultaneously.

During T2, as U_∞ is slowly increased, there is no significant change in the amplitude of both heaving and pitching displacement.

During T3, after U_∞ has reached 16.81 m/s, the vibration amplitude starts to grow, as observed from Fig. 3(c) and Fig. 3(d). This condition is called flutter and the flutter speed $U_F = 16.81$ m/s and flutter frequency was found to be 3 Hz.

During T4, as U_∞ is slowly decreased to 15.74 m/s, the vibration amplitude still remains the same.

During T5, after U_∞ has reached 15.74 m/s, the vibration amplitude starts to decrease.

In summary, amplitude starts to grow after U_∞ has reached 16.81 m/s. This speed at which the amplitude starts to grow is called the flutter speed (U_F). For the present aeroelastic system $U_F=16.81$ m/s. In the left neighborhood of U_F the system encountered intermittent oscillations during which the oscillations grew and decay irregularly.

In order to understand further, detailed analysis of the aerodynamic forces and the wing section motion is considered. Figure 4 shows the zoomed in view of heaving displacement and pitching displacement in time interval $283 \leq t \leq 285$. Consider one cycle of motion (as marked in Fig. 4(a) and 4(b)) which are further expressed as “forward-path” and “reverse-path”. In Fig. 4(a), the path 1-2 represents the part of cycle during which, linear displacement (h) of the wing section is along the direction of Lift (L); called “forward-path” and path 2-3 represents the part of cycle during which the linear displacement (h) of the wing section is opposite to the direction of the Lift (L); called “reverse-path”. In Fig. 4(b), path 1-2 represents the part of cycle during which the angular displacement (ϕ) of the wing section is along the direction of Moment (M); called “forward-path” and path 2-3 represent the part of cycle during which angular displacement (ϕ) of the wing section is opposite to the direction of the Moment (M); called “reverse-path”.

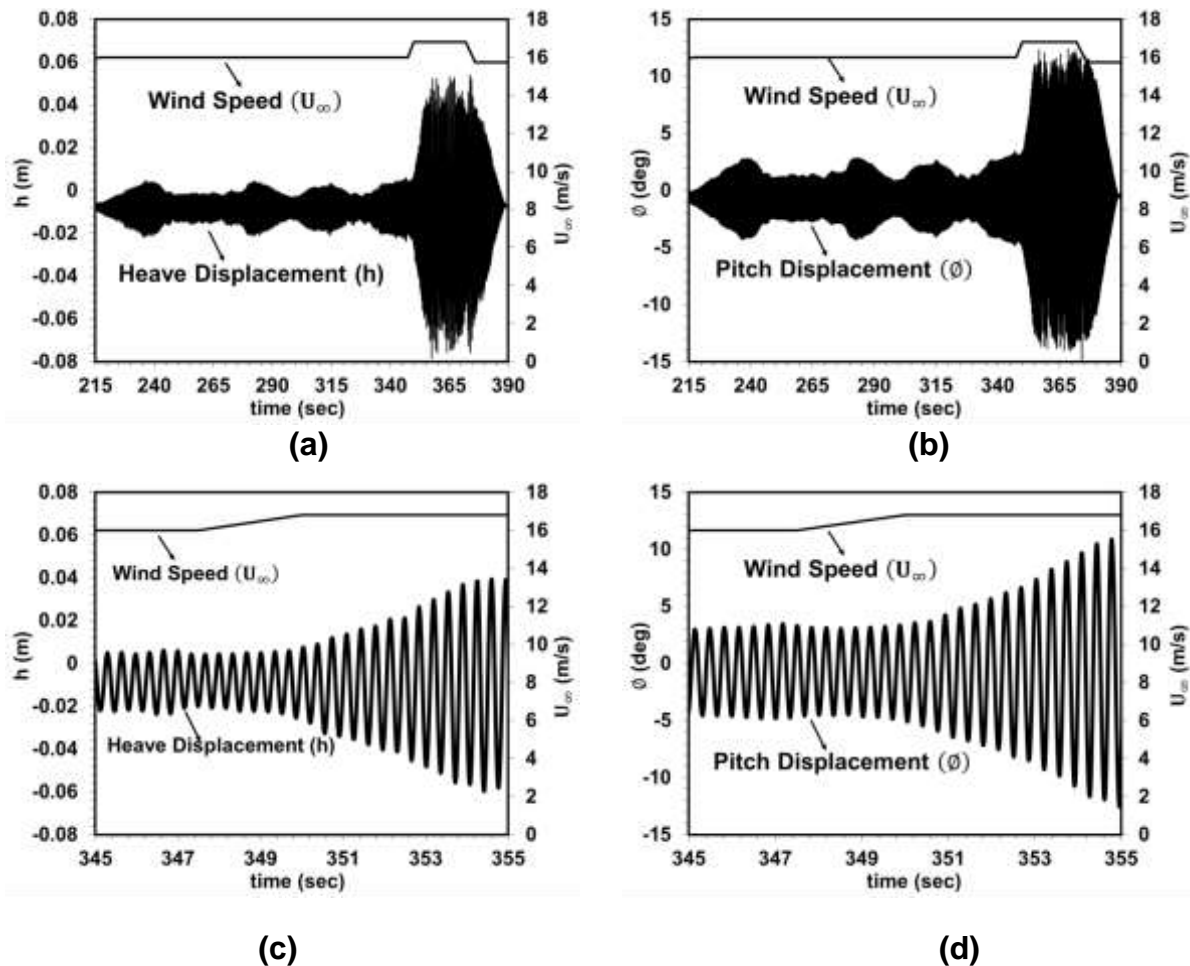


Fig. 3 Behavior of (a) Heaving displacement (b) Pitching displacement in Time of Interest (c) Heaving displacement (d) Pitching displacement in $345 \leq t \leq 355$

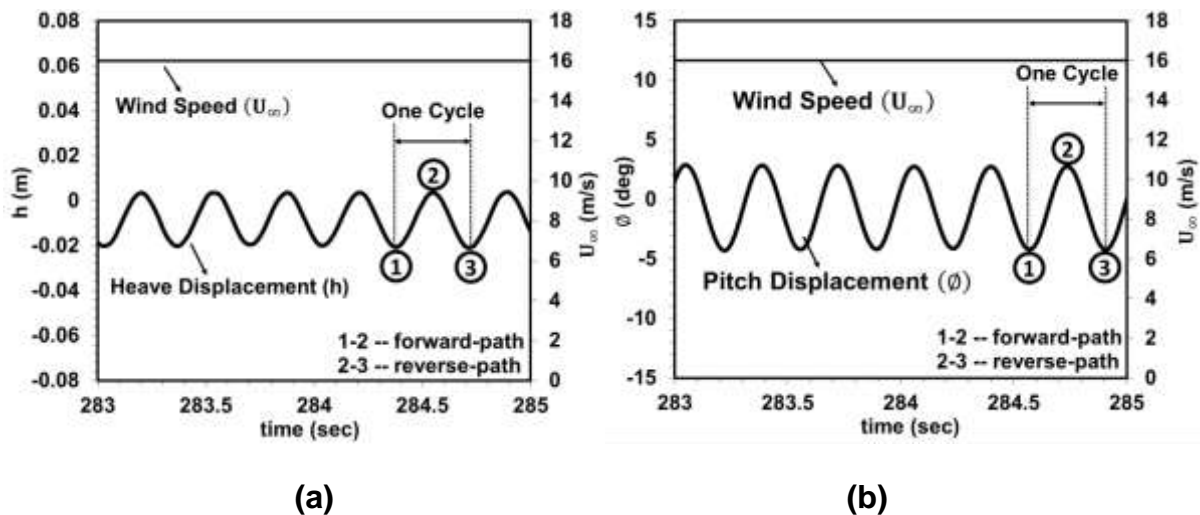


Fig. 4 Behavior of (a) Heaving displacement (b) Pitching displacement in $283 \leq t \leq 285$

To understand the reasons behind the above mentioned behavior of the wing section (as explained in Fig. 3), an in-depth insight into the aerodynamic parameters during the one cycle of motion (as mentioned in Fig. 4) at different U_∞ is required.

Since the lift (L) is the cause for linear displacement (h) and moment (M) is the cause for pitching displacement (ϕ), consider the behavior of lift (L) with heaving displacement (h) and moment (M) with pitching displacement (ϕ), which is shown in Fig. 5.

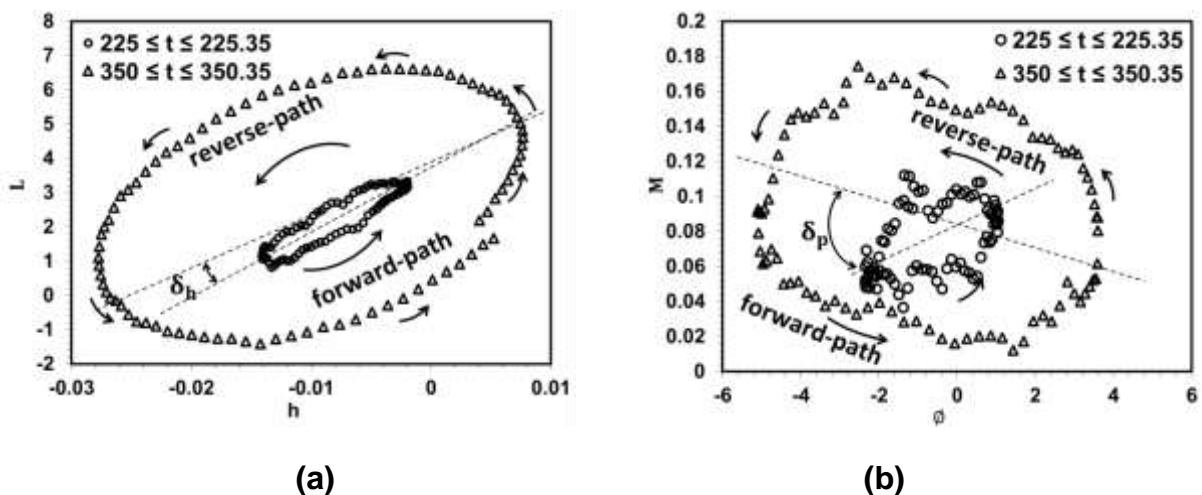


Fig. 5 Behavior of (a) Lift with heaving displacement (b) Moment with pitching displacement for $225 \leq t \leq 225.35$ and $350 \leq t \leq 350.35$

Figure 5(a) shows the behavior of lift (L) with heaving displacement (h) and Fig. 5(b) shows the behavior of moment (M) with pitching displacement (ϕ) for one cycle of

motion at two different U_∞ 's, namely 16 m/s ($225s \leq t \leq 225.35s$) and 16.81 m/s ($350s \leq t \leq 350.35s$). The dashed lines denote the axis of symmetry. From both these plots the following features are observed. First, forward-path and reverse-path are different for both lift (L) and moment (M) forming elliptic loops, for both the time intervals. As the forward-path and reverse-path are different, the system is said to exhibit hysteresis, and the loop is known as "hysteresis loop". Second, the direction of loop is counter clock-wise for both Lift and Moment at both the time instants. Third, as U_∞ is changed (increased), the orientation of the hysteresis loop gets modified (by ' δ_h ' for heaving displacement and ' δ_p ' for pitching displacement) as indicated.

In order to understand the possible reasons for the hysteresis, and the change in its behavior, the following analysis is carried out for using a classical vibration system. Reconsider Eq. (1) replacing $F(t)$ with $F_0 \sin \Omega t$ resulting in Eq. (5).

$$m\ddot{X} + c\dot{X} + kX = F_0 \sin \Omega t \quad (5)$$

For $\Omega \neq \sqrt{\frac{k}{m}}$, consider the behavior of the external force ($F(t)$) with ' X '. Figure 6(a) shows the behavior of $F(t)$ with ' X ' during one cycle of vibration for both $c = 0$ and $c > 0$. From the plot, the following can be observed. For the case with $c = 0$, the forward-path and reverse-path are same, whereas, for case with $c > 0$ (or $c < 0$ shown in Fig. 6(b)), the forward-path and reverse-path are different, forming an elliptic loop (called "hysteresis-loop"). This is same as observed in Fig. 5(a) and 5(b). From this, it can be asserted that the damping (' c ') is the reason for the hysteresis in vibrating systems.

Figure 6(b) shows the behavior of $F(t)$ with $X(t)$ during one cycle of motion with $c < 0$ and $c > 0$. From the plot, the following are observed. First, the loop direction gets reversed (from counter clock-wise to clock-wise) as the sign of ' c ' changes (from positive to negative). Second, the orientation of the elliptic loop changes (by δ) with change in magnitude of ' c ' (magnitude of ' c ' for Path2 is higher than the magnitude of ' c ' in Path1).

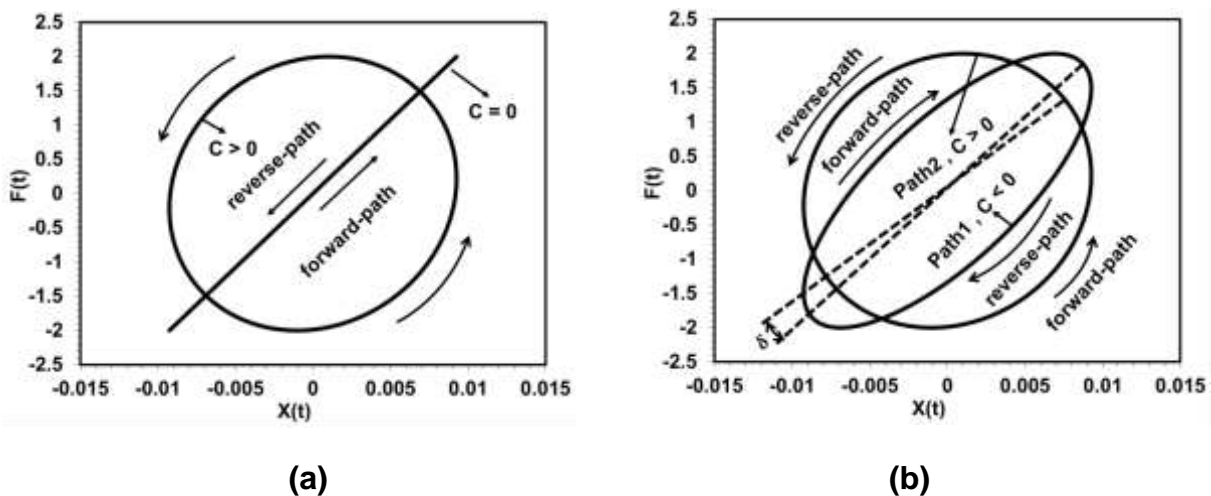


Fig. 6 Behavior of force with displacement for (a) $c = 0, c > 0$ (b) $c < 0, c > 0$

Based on the observations from Fig. 5 and Fig. 6 the following conclusions can be drawn. During the oscillation of the wing section, lift (L) and moment (M) form an elliptic loop with respect to their respective displacements called the hysteresis loop. As U_∞ is varied, the orientation of the hysteresis loop gets modified. On comparing to the observations from Fig. 6 the change in the orientation of the hysteresis loop can be attributed to the change in damping coefficient ('c'). When the damping due to U_∞ is equal to the structural damping already associated with the system, the overall damping of the system approached zero, the oscillation amplitude grows monotonically with time. This situation is called flutter.

From above, it can be concluded that the change in behavior of the hysteresis loop leads to the system to flutter.

4. CONCLUSIONS

Wind tunnel testing of an aeroelastic model of a wing section, instrumented with surface pressure taps was carried out. In addition to the surface pressure, the motion of the position and orientation of the wing section was computed using the image captured using video camera. Based on the behavior of the lift (L) with heaving displacement and behavior of moment (M) with pitching displacement, it was observed that the aeroelastic system exhibited hysteresis. As the wind speed was increased, the orientation of the hysteresis loop changes and the system enters flutter. On comparison with the classical vibration system, change in orientation of the hysteresis loop can be associated with the change in the damping coefficient.

REFERENCES

- Bollay, W., and Brown, C. D. (1941), "Some Experimental Results on Wing Flutter", *Journal Aeronautical Sciences*, **8**(8), 313-318.
- Lee, T., and Gerontakos, P (2004), "Investigation of flow over an oscillating airfoil", *Journal of Fluid Mechanics*, 512, 313-341.
- Sekar, T. C., Agarwal, R., Mandal, A. C., and Kushari, A. (2017) "Behavior of an aeroelastic system beyond critical point of instability", *Physics of Fluids*, **29**(11), 114103-114119.
- Strogatz, H.S. (2007), "Bifurcations Revised," *Nonlinear Dynamics and Chaos*, **Chapter 8**, 248-254.
- Theodorsen, T. (1949) "General theory of aerodynamic instability and the mechanism of flutter," NACA Report No. 496.